

Effects of surface roughness on liquid bridge capillarity and droplet wetting

Hien Nho Gia Nguyen^a, Chao-Fa Zhao^{b,*}, Olivier Millet^a, A.P.S. Selvadurai^c

^a LaSIE-UMR CNRS 7356, Université de La Rochelle, 23 Avenue Albert Einstein, La Rochelle 17000, France

^b Faculty of Engineering Technology, University of Twente, P.O. Box 217, Enschede 7500 AE, the Netherlands

^c Department of Civil Engineering and Applied Mechanics, McGill University, Canada

ARTICLE INFO

Article history:

Received 25 June 2020

Received in revised form 13 September 2020

Accepted 5 October 2020

Available online 08 October 2020

Keywords:

Surface roughness

Liquid bridge

Young-Laplace equation

Capillary force

Droplet wetting

ABSTRACT

This study examines the influence of surface roughness on the capillarity of liquid bridges between two solid surfaces and the wettability of droplets on solid surfaces. For this purpose, different surface roughnesses were prepared by gluing waterproof sandpaper onto flat glass surfaces. The effects of surface roughness on liquid bridge capillarity were investigated by using a method that is based on an exact analytical solution of the Young-Laplace equation for a liquid bridge between two parallel planes coupled with capillary force measurement. The capillary forces between two parallel planes were measured by a micro-balance, while the geometries of the capillary bridge were recorded using a high-resolution camera. Using the images of capillary bridges, the meridional profiles of capillary bridges were determined by a high-resolution image processing technique and correlated to the measured capillary forces. The effects of surface roughness on droplet wetting were measured by employing the same high-resolution image processing technique. The measured results show that as the roughness increases, the wetting angle increases, whereas the capillary forces of the liquid bridge decrease.

© 2020 The Author(s). Published by Elsevier B.V. This is an open access article under the CC BY license (<http://creativecommons.org/licenses/by/4.0/>).

1. Introduction

Water in the pore space exerts a significant influence on the mechanical behavior of granular materials and powders. At the micro-scale, the liquid menisci formed between two adjacent solids create an attraction force due to the presence of a capillary bridge. This physical phenomenon has an important role in many fields in the engineering sciences, ranging from powder technology, flow of particles, to friction between surfaces [1,2]. Several methods can be used to estimate the capillary attractive force including direct measurement using a micro-balance, an exact analytical solution of the Young-Laplace equation derived from experimental data [3], or some approximations of the shape of the capillary surface [2,4–7]. In general, the theoretical approaches rely on a knowledge of the Young-Laplace equation, which considers the air-liquid interface to have a constant mean curvature [8,9].

Surface roughness brings an added level of complexity to this problem, since different roughnesses affect the wettability of a liquid; this is of interest to many scientific and engineering applications, for example coating, waterproofing, painting, fluid flow, etc. [10–12]. The wettability of a liquid on a solid surface is, in fact, linked directly to the contact angle, which is determined by contact processes between the fluids and a surface at the three-phase line.

The form of the liquid bridge profile depends on several geometrical boundary conditions, including the contact angle. In theory, the contact angle (denoted hereafter by θ_r), is a unique value for a given solid-liquid-air group. In practice, this value may vary, depending on various conditions including relative humidity, the property of the solid surface, the purity of the liquid, movement of the contact line (hysteresis phenomenon [13–16]). Studies of capillary bridges usually consider a smooth surface for simplicity. However, this consideration renders an ideal state, which is difficult to replicate, since in reality, surface roughness always exists, even if it is at a (very) low level. In analytical studies, researchers usually consider ideally smooth surfaces, leading to difficulties when attempting to compare these solutions with experimental validations.¹ The same factors have to be taken into account in computational simulations of granular media using the Discrete Element Method (DEM) or averaging method, where the surface of a body is considered perfectly smooth [17–22]. In experimental studies of capillary bridging, the surfaces with the least roughness are used, because of the ease of experimental preparation and measurement [23–25].

There have been several studies on surface roughness and capillarity, including [26]. When the effect of surface roughness is taken into account, the contact angles on the rougher solids are greater when the

* Corresponding author.

E-mail address: c.zhao-1@utwente.nl (C.-F. Zhao).

¹ In theory, the contact angle for a set comprising solid-air-liquid is unique. However, in reality the contact angle varies depending on the surface property and the direction of the contact line movement (advancing or receding).

droplets are on flat surfaces [27,28]. The difference between the contact angles results in asymmetrical capillary bridges [29]. However, only a few studies have concentrated on how the surface roughness affects the capillary force and the geometrical form of the capillary bridge meniscus. The influence of surface roughness on capillary forces was addressed in [30] and an analytical method to calculate the capillary force between two undeformable spheres with various levels of roughness has been proposed. However, a direct link between the capillary force, the surface roughness and the description of the shape of the capillary bridge is yet to be found.

This paper aims to elucidate the effect of surface roughness on the capillary force and the properties of the capillary bridges. Two main topics are investigated: the description of the meridian of the capillary bridge and the variation of the corresponding capillary force under different levels of surface roughness. In the following, the theory of a capillary bridge between two solids is revisited. The theoretical analysis is followed by an experimental section, where tests of capillary bridges between surfaces with different roughness are performed. In each test, the capillary force is measured and the associated profile of the capillary bridge is analyzed using an image processing technique. In the final section, in order to obtain a complete observation of the impact of surface roughness on the wettability of surfaces, supplementary tests of droplets on inclined planes with different roughness levels were performed. This study will complete the existing research reported in [27,28,30–33].

2. Geometry of a capillary bridge and the Young-Laplace equation

2.1. Analytical solution of the Young-Laplace equation for a capillary bridge between two solids

It is well known that for a static capillary bridge formed by an inviscid fluid between two adjacent solids, the mean curvature and the suction are governed by the Young-Laplace equation [2,3,9]. Moreover, knowing the description of the meridional profile of the capillary bridge, one can easily deduce the corresponding capillary force for a given liquid.

Let us consider capillary bridges between two adjacent solids (poly-disperse spheres, sphere-plate or plate-plate²), in a two-dimensional Cartesian coordinate system Oxy , as described in Fig. 1. The axial coordinate is denoted by x , while the meridional profile of the liquid bridge is denoted by $y(x)$. The origin corresponds to the neck of the liquid bridge.

The surface of the axisymmetric capillary bridge can be considered as a surface of revolution described by a constant mean curvature H_r , satisfying the Young-Laplace equation. In the absence of gravity, it can be written as

$$\frac{y''}{(1+y'^2)^{3/2}} - \frac{1}{y(1+y'^2)^{1/2}} = -\frac{\Delta p_r}{\gamma} = H_r, \quad (1)$$

where Δp_r is the pressure difference between the liquid phase and the air phase, γ is the surface tension of the liquid and $x \mapsto y(x)$ describes the upper profile of the capillary bridge. The integration of the Young-Laplace equation yields the non-linear first order differential equation [3],

$$1 + y'^2 = \frac{4y^2}{H_r^2 \left(y^2 - \frac{2\lambda_r}{H_r} \right)^2} \quad (2)$$

with $\lambda_r = \frac{y}{\sqrt{1+y'^2}} + \frac{H_r y^2}{2}$.

² Note that the plane-plane case can be viewed as a particular case of a capillary bridge between two spheres by simply considering $r \rightarrow \infty$, where r is the radius of the sphere.

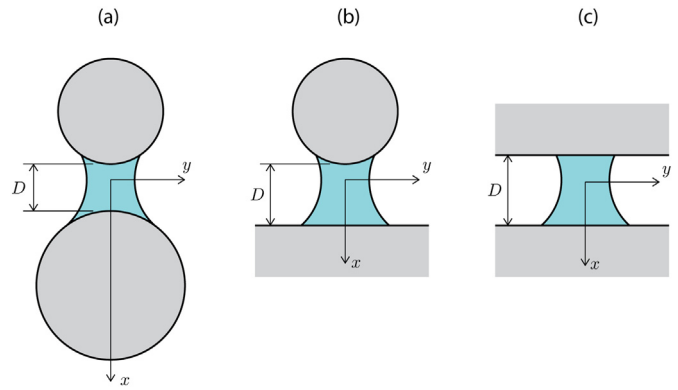


Fig. 1. Schematic representation of an axisymmetric concave capillary bridge between two solids with a convex meridional profile: definition of the coordinate system.

It is noted that the mean curvature and the pressure difference in this study are denoted by H_r and Δp_r , respectively. The surface roughness has a substantial influence on the boundary condition of the liquid bridge, even for the same geometric configuration (identical liquid volume V and separation distance D). In other words, H_r and Δp_r vary according to the level of surface roughness. Section 3.3 will discuss the impact of surface roughness on the liquid bridge properties in detail.

Depending on the signs of H_r and λ_r , Eq. (2) expresses a form similar to the Delaunay roulettes [34]

$$1 + y'^2 = \frac{4a^2 y^2}{(y^2 + \varepsilon b^2)^2}, \quad (3)$$

the corresponding surface of revolution being a portion of nodoid (for $\varepsilon = -1$) or unduloid (for $\varepsilon = 1$). The parameters $a = \frac{1}{|H_r|}$ and $b^2 = \left| \frac{2\lambda_r}{H_r} \right|$ can be calculated from geometrical data of the liquid bridges, which will be discussed in the following subsection.

2.2. Exact description and classification of capillary bridges between two parallel planes as an inverse problem from experimental data

This subsection introduces the exact solution of the Young-Laplace equation for the case of capillary bridges between two identical smooth parallel planes, where the effect of gravity is neglected. This theoretical result will be used to analyze the results of experiments described in Section 3. For the case of rough surfaces, the boundary conditions may change (contact angle θ_r and contact radius y_c); however, the general

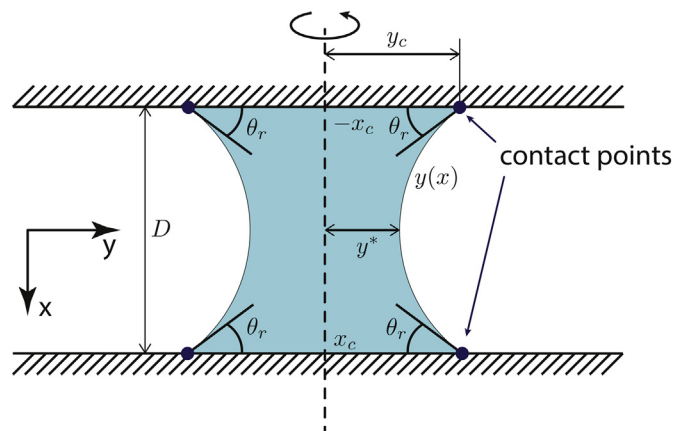


Fig. 2. Schematic illustration of an axisymmetric capillary bridge between two parallel planes.

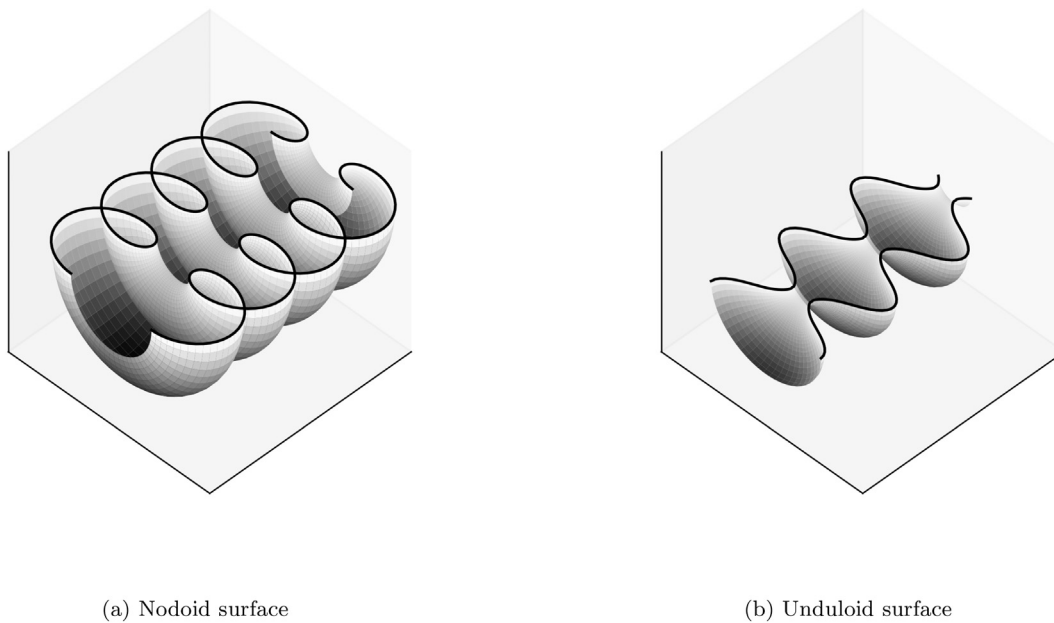


Fig. 3. Examples of nodoid and unduloid surfaces. Only half of the surfaces are shown in order to display the internal structure as well as the profile of the revolution.

theory describing the capillary surface remains the same as those developed in [35]. The surface roughness greatly influences the wetting angle θ_r in particular, as we will see in the Sections 3 and 4.

Following the theoretical approach proposed in [3], for sufficient measured data from the geometry of a real capillary bridge, the associated meridional profile can be recovered from the solution of the Young-Laplace equation based on an inverse problem. The measured data includes the neck radius y^* , the contact angle θ_r , and the contact radius y_c (Fig. 2). From a classification that is only based on (y^*, θ_r, y_c) , the surface of the captured capillary bridge can be classified into portions of either a nodoid or an unduloid with other limit cases (catenoid, sphere, cylinder, etc.; see [35] for more details). Illustrations of nodoid and unduloid surfaces of revolution are shown in Fig. 3.

We recall here the main results for the nodoid and unduloid cases that will be used later in the experimental analysis. When the measured data of the liquid bridge satisfy the condition

$$y_c \sin \theta_r < y^* < y_c, \tag{4}$$

the surface of the capillary bridge is a portion of a nodoid surface. The convex profile is described by the parametric equations

$$\begin{cases} x(t) = \frac{b^2}{a} \int_0^t \frac{\cos u du}{(e + \cos u) \sqrt{e^2 - \cos^2 u}} \\ y(t) = b \sqrt{\frac{e - \cos t}{e + \cos t}}, \quad t \in [-\tau, \tau] \end{cases} \tag{5}$$

where τ is unique and determined from $\tau = \arccos\left(e \frac{b^2 - y_c^2}{b^2 + y_c^2}\right)$. The eccentricity e is calculated as $e = \frac{\sqrt{a^2 + b^2}}{a}$, where a and b are the parameters defined by

$$\begin{aligned} a &= \frac{1}{2} \frac{y_c^2 - y^{*2}}{y^* - y_c \sin \theta_r} = \frac{1}{H_r}; \\ b^2 &= y^* y_c \frac{y_c - y^* \sin \theta_r}{y^* - y_c \sin \theta_r} = \frac{2\lambda_r}{H_r}. \end{aligned} \tag{6}$$

Otherwise, if the geometry of the capillary bridge meets the criterion $0 < y^* < y_c \sin \theta_r$,

the meridional profile of the capillary bridge is convex and its revolution around the x -axis is a portion of an unduloid surface. In accordance with

the experimental results presented in this paper, only stable capillary bridges (whose profiles are portions of a nodoid surface) are addressed. For the sake of simplicity, the parametric equation for the case of an unduloid portion is not introduced.

In both cases, the associated capillary force can be calculated from

$$F^{cap} = 2\pi\gamma\lambda_r, \tag{8}$$

where λ_r corresponds to the first integral of the Young-Laplace equation given in Eq. (2). Therefore, it is constant on the profile and can be calculated at any point. At the neck, corresponding to $y(0) = y^*$ and $y'(0) = 0$, F^{cap} reduces to the classical expression

$$F^{cap} = 2\pi\gamma y^* + \pi\gamma H_r y^{*2}, \tag{9}$$

which was referred to as the “gorge method” in [3,9].

From experiments, using an image processing technique on high resolution photographs of capillary bridges, y^* can be measured directly from the meniscus profiles and H_r can be calculated from the exact analytical solution of the Young-Laplace equation with precisely measured boundary condition using Eq. (6), as described in [36].

It should be noted that the above calculation is applied to a smooth surface, where the contact angle at the boundary is constant. However, different surface roughness profiles can have a significant influence on its wettability. This requires a change to the way the contact line³ behaves on the surface. These variations directly change the boundary conditions used to develop the analytical solution of the Young-Laplace equation. In the following section, experiments between parallel planes of the same materials and different surface roughnesses were performed to reveal this phenomenon.

3. Measuring the effects of surface roughness on liquid bridge capillarity

3.1. Experimental set-up

The experimental facility consists of two parallel planes, a weighing system and an image acquisition system (Fig. 4). Waterproof sand paper of different grit grading was glued to the surface of the plane to change its roughness. The two planes were positioned horizontally and parallel:

³ Three-phase boundary

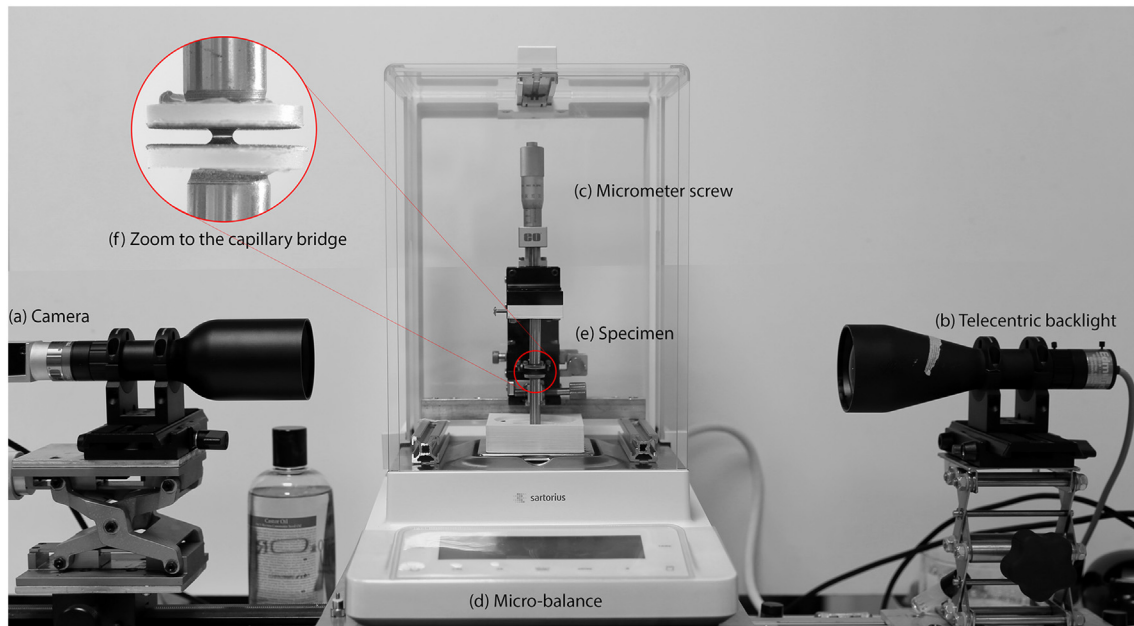


Fig. 4. Set-up of the experimental apparatus: (a) image acquisition system, (b) telecentric backlight, (c) micrometer-screw to control the separation distance, (d) micro-balance to measure the experimental capillary force F_{exp}^{cap} , (e) specimen, (f) capillary bridge between two planes.

the lower plane was fixed on a micro-balance (Sartorius MCE225P) with a precision of 0.01 mg , and the upper plane was controlled by a micrometer screw, assuring uniform movement along the vertical direction with a precision of 0.01 mm . The image acquisition system includes a high-resolution camera (Basler-acA4600) coupled with a telecentric back-light. The micro-balance provides the value of the experimental capillary force F_{exp}^{cap} . All tests were carried out under identical environmental conditions in a temperature and humidity controlled laboratory.

In each test, a small predefined volume of water ($2\ \mu\text{l}$) was injected between the two plates and a capillary bridge was formed. For each separation distance D , the value of the experimental capillary force was measured. The micro-balance requires a period of about 5 s to be stabilized and to provide the output of F_{exp}^{cap} . Once the value of F_{exp}^{cap} was obtained, a unique image of the capillary bridge was recorded. Then, the upper plate was moved upward $\Delta d = 0.05\text{ mm}$ and a new recording-weighing process was carried out. The test was terminated when the capillary bridge broke.

Different surfaces were prepared by gluing emery paper (also known as sand paper) directly onto the smooth glass planes. In the experiments, waterproof sand paper of different roughnesses was used; ranging from very rough to smooth: P80 (very rough), P180, P320, P600, P1000, P2000, P3000 (smooth). The corresponding grit sizes are presented in Table 1.

The experimental protocol is described as follows. The lower plane was fixed on the micro-balance, and the upper plane was moved vertically using a micro-meter screw with movement precision of 0.01 mm . Distilled water was injected between the two planes using a micro-syringe with a precision of $0.01\ \mu\text{l}$. A fluid volume of $2\ \mu\text{l}$ was used in order to avoid the effect of gravity on the form of the capillary bridge. This amount was chosen to conform to the Bond number Bo proposed in [37,38] as an indicator to estimate the effect of gravity on the shape of the liquid bridge distortion, to be small in comparison to unity.

The capillary force was measured directly by a precise micro-balance with a precision of 0.01 mg . The balance was set to zero (tare) just before injecting the water between the two plates. The value given by the balance includes the weight of the liquid quantity and the capillary force. Hence, for a given capillary bridge, F_{exp}^{cap} can be calculated by $F_{exp}^{cap} =$

Table 1

Grit size table of the sandpapers used in the experiments.

Surface type	Sandpaper grade	Average particle diameter (μm)
Very rough	P80	201
Rough	P180	82
Rough	P320	46.2
Rough	P600	25.8
Rough	P800	21.8
Rough	P1000	18.3
Smooth	P2000	10.3
Smooth	P3000	7

$\rho V_w - M$ where ρ is the density of water, V_w is the actual water volume at the time of measurement, M is the output of the balance (and V_w is calculated once the profile of the capillary bridge is recovered from image processing).

A high resolution camera (BASLER acA4600 $10\ \mu\text{m}$) was used to photograph the liquid bridges. The output images were processed using *ImageJ* and *MATLAB* software was used to recover the geometry data for the liquid bridge: the gorge radius y^* , contact angle θ_r , and contact radius y_c . Some relevant horizontal views of different surface roughness levels are shown in Fig. 5.

3.2. Image processing procedure

The image acquisition and analysis procedure was performed in the following steps:

- A sequence of photographs of the capillary bridge was obtained in B/W format, from a near-touching state to the breakage of the liquid bridge.
- Then, by using the *threshold* utility in *ImageJ*, the contour of the bridges and the boundary in the photographs was traced to visualize accurately the capillary bridge profile and the two planar surfaces, as well as for the detection of the contact points.
- Finally, using the obtained geometrical measurement of wetting angles θ_r , neck radius y^* , and contact radius y_c , the numerical capillary

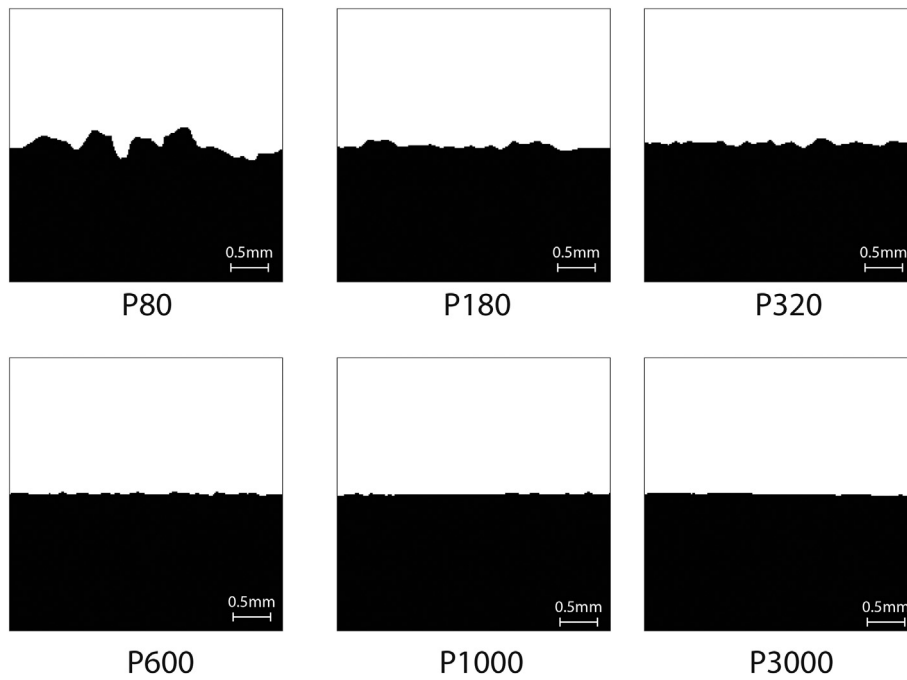


Fig. 5. Side views of surfaces with different roughness levels.

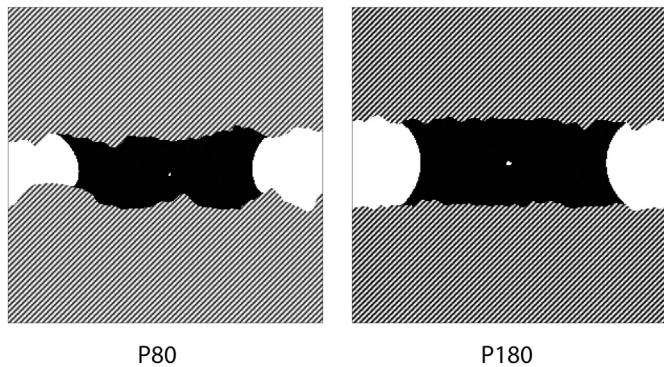


Fig. 6. Capillary bridges between two rough parallel plates, cases of P80 and P180. The surface is highlighted with the striped pattern.

bridge profile was recovered from Eq. (5) and superimposed on the experimental photos for validation purposes.

For all the tests, the same amount of water $V = 2 \mu\text{l}$ was used.⁴ This amount of liquid has been verified to be unaffected by gravity (see [25,38,39]). Identical laboratory conditions were maintained at $T = 20^\circ\text{C}$. The capillary forces generated between parallel planes of P80, P180, P320, P600, P800, P1000, P2000, and P3000 were measured and compared with each other. As mentioned in previous studies [3,25], when the separation distance is gradually increased, the profile of a capillary bridge follows the common sequence: nodoid – catenoid – unduloid – rupture. However, in this study, only the nodoid profiles of capillary bridges were analyzed as the micro-balance cannot provide a stable output of F_{exp}^{cap} for the unduloid configuration. Indeed, during the stabilization of the micro-balance, the liquid bridge cannot maintain a stable form and is broken in the unduloid stage.

We also note that the P80 and P180 surfaces are omitted for image processing and comparison with the theory, since the grit size of the

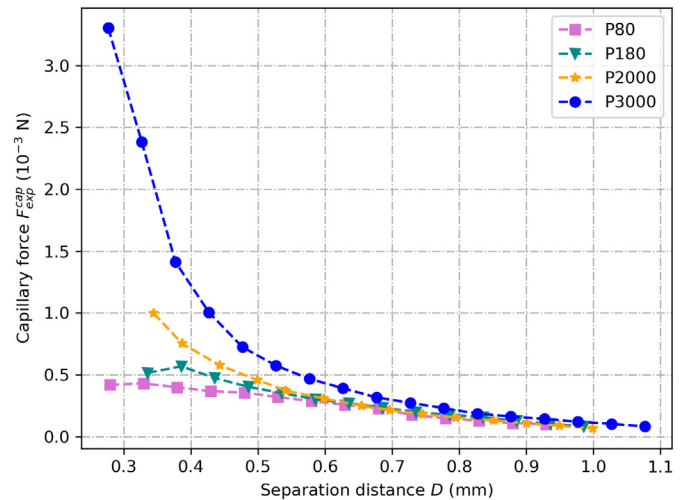


Fig. 7. Variation of the measured capillary force F_{exp}^{cap} for different surface roughness levels.

emery papers was too large, making it impossible to estimate accurately the contact angle by image processing (Fig. 6). Nevertheless, we were able to measure the associated capillary force with the micro-balance, as explained previously.

3.3. Effects of surface roughness on liquid bridge capillarity

Following the experimental protocol presented in the previous sections, we focus on the variation of capillary forces (measured from a high precision balance) with respect to the roughness of the surfaces. It is shown that the values given by different roughness levels share the same tendency with the “smoothness” of the surface (see Fig. 7). The emery papers considered were P80, P180, P1000, and P3000 (from rough to smooth following Table 1). Fig. 7 shows that the capillary force tends to be greater for smooth surfaces. For the same testing configuration and the same separation distance, the smoothest surface

⁴ Volume controlled configuration.

provides the maximum capillary force. In contrast, for the roughest surface P80, the value of F_{exp}^{cap} is the smallest.

As mentioned in section 2.1, when γ is constant, the capillary force depends on the variation of the mean curvature H_r , which is directly connected to the contact angle θ_r , and the value of the neck radius y^* . In the following sections, depending on the complexity of the surface and feasibility of performing image processing techniques, a subset of surfaces was selected and used for further analysis.

The procedure of image processing is similar to that used in [23,36], enabling a comparison of the numerical curve, based on the exact analytical solution of the Young-Laplace equation from the inverse method, with the experimental images. We limit our analyses to the most relevant surfaces that had emery papers P320, P2000, and P3000. In each comparison, the variation of the contact angle θ_r , neck radius y^* , and mean curvature H_r are shown.

As presented in Figs. 8, 9 and 10, the smoother surface yields greater values for the mean curvature, neck radii and contact radius until a separation distance of about $D = 0.75$ mm. In particular, as seen in Figs. 8 and 9, at the same separation distance D , different roughnesses cause a difference in the mean curvatures and neck radii. Consequently, according to Eq. (9), the resulting capillary force differs. However, the contact angle (Fig. 11) has the contrary tendency: rougher surfaces render greater values of the contact angle θ .

In Fig. 12, from Eq. (9), the two components $F_1^{cap} = 2\pi\gamma y^*$ and $F_2^{cap} = \pi\gamma H_r y^{*2}$ of the total capillary force are plotted, where $F_1^{cap} = 2\pi\gamma y^*$ is the surface tension resulting force and $F_2^{cap} = \pi\gamma H_r y^{*2}$ is the pressure resulting force [9,38]. F_1^{cap} depends only on the variation of the neck radius y^* , whereas F_2^{cap} depends on both y^* and H_r and its variation is more complex. It is shown that the pressure resulting force acts as the main source for the total capillary force. For the same roughness level, F_2^{cap} is almost ten times larger than F_1^{cap} .

In order to investigate accurately the variation of the neck radius y^* for a higher value of the separation distance $D > 0.75$ mm, images of different experiments performed for P600, P800, P1000, P2000 and P3000 at a similar separation distance D were selected and compared. Two D -ranges were selected: (1) Medium D (intermediate state): 0.72 mm – 0.75 mm, (2) Large D (ultimate state): 0.98 mm – 1.04 mm. The comparison between different surfaces is shown in Fig. 13.

It was observed that starting from $D \approx 0.75$ mm there was an inverse tendency, i.e. when the surface gets rougher (grit size increases), y^* increases accordingly. However, according to the small gap between y^* , this tendency must be checked more accurately. This was already visible in the results on the right hand part of Fig. 10 for values of D larger than 0.75 mm.

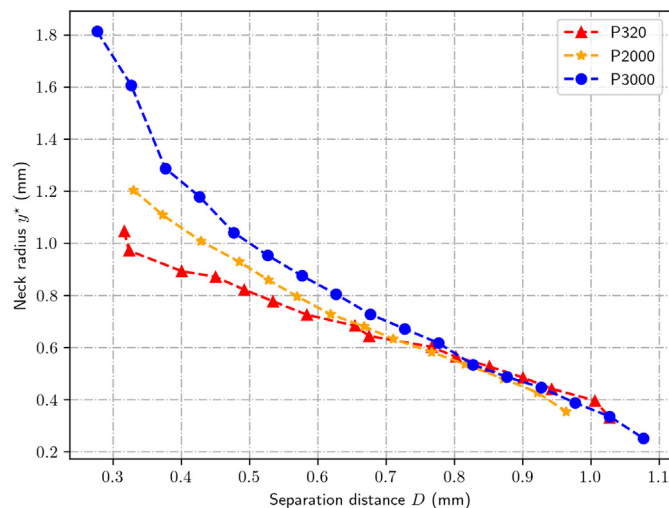


Fig. 8. Variation of the neck radius y^* in terms of separation distance.

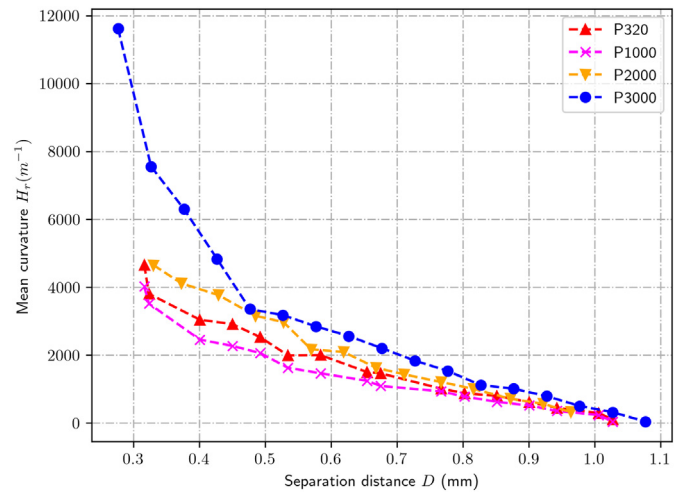


Fig. 9. Variation of the mean curvature in terms of separation distance.

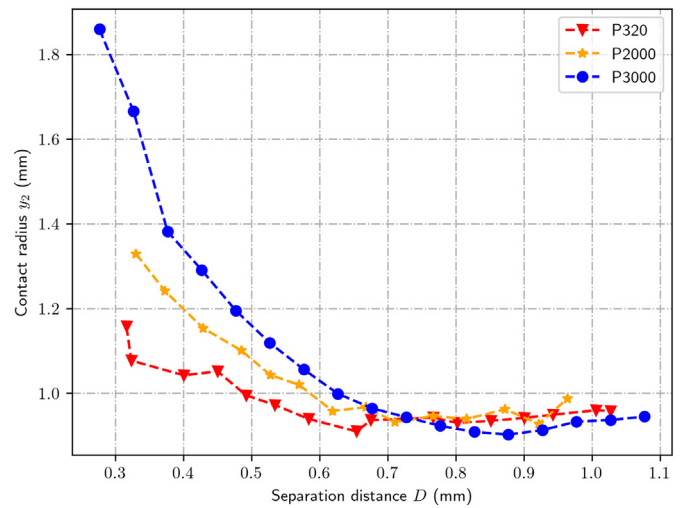


Fig. 10. Variation of the contact radius in terms of separation distance.

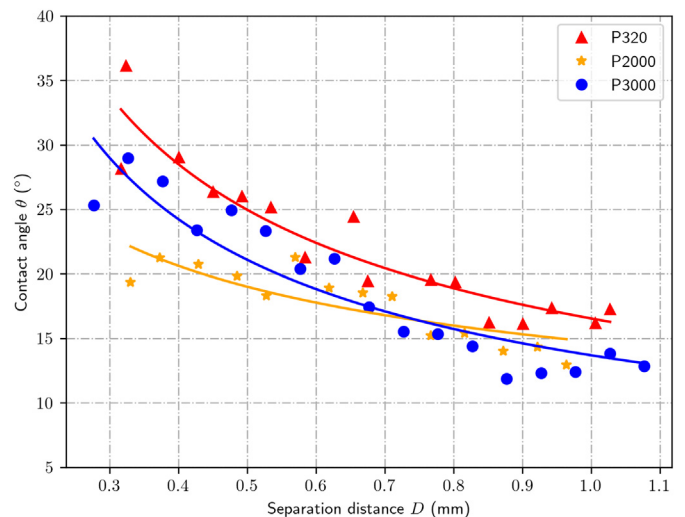


Fig. 11. Variation of the contact angle in terms of separation distance.

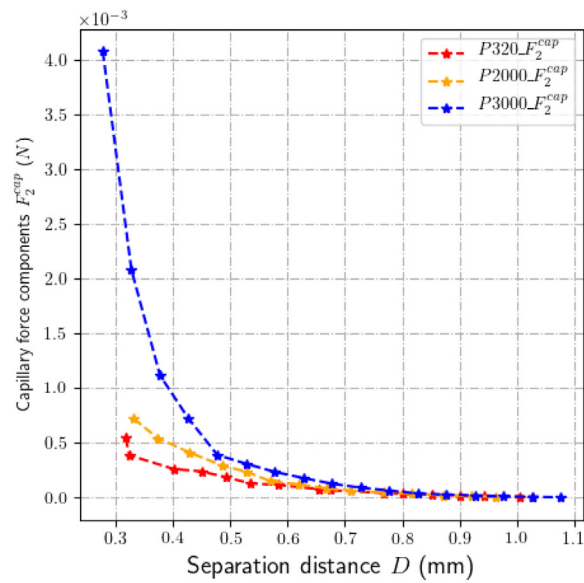
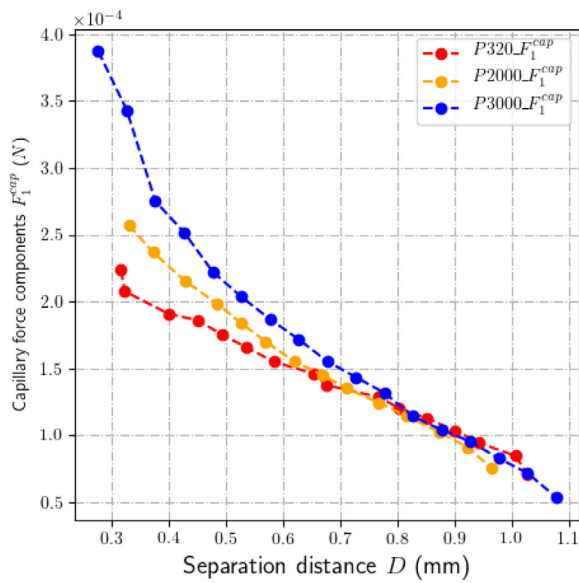


Fig. 12. Variation of the components of F^{cap} in terms of separation distance. $F_1^{cap} = 2\pi\gamma\gamma^*$ and $F_2^{cap} = \pi\gamma\gamma^*H_r$.

4. Measuring the effects of surface roughness on droplet wetting

4.1. Droplets on a rough inclined solid surface

In this section, several tests of droplets on inclined surfaces of different roughness were performed to investigate the impact of the surface property on the spreading ability of a liquid, also known as wettability, which is a well-known indicator to define the spreading action of a liquid on a solid surface. Depending on the properties of the surface material, the surface may be considered as hydrophobic or hydrophilic. For surfaces that have a hydrophobic property (such as Teflon, wax-covered surfaces, etc.), the droplet tends to reduce the contact surface and yield large values of the contact angle. On the other hand, for a hydrophilic surface (e.g. glass), the droplet can spread easily and the contact angle is smaller. Changing the degree of the surface roughness may lead to similar behavior. Studying the forms of droplets on different surface roughnesses is a convenient and direct way to demonstrate how the contact angle changes according to the surface properties. It has been stated that contact angles, as well as the hysteresis of wetting,

appear to be greater for rougher surfaces (e.g. [27]). Rough surfaces also affect the rebounding performance of a droplet impacting them, see for instance [40]. For the case of a regular flat surface, some studies [33] were performed on metal and ceramic surfaces limited to nil angle of inclination.

When a static droplet is formed on a horizontal flat surface, it is possible to estimate the contact angle at the triple line based on image analysis. The necessary data includes the baseline, the edge of the droplet and the tangent vector to the edge defined from data points of the edge of the droplet. In this procedure, the droplet is axisymmetric and consequently the measured contact angle is constant along the triple line. However, once the surface is inclined, the droplet deforms due to the effect of gravity (Fig. 14) and variations in the contact angle are observed. Along the distortion direction, two values θ^+ and θ^- can be taken into account for investigation, $\theta^+ > \theta^-$. The contact angles θ^+ , θ^- are also known as the advancing and receding contact angles, respectively (for example, see [41]). It is convenient to perform tests of droplets on inclined surfaces where both advancing and receding angles can be observed.

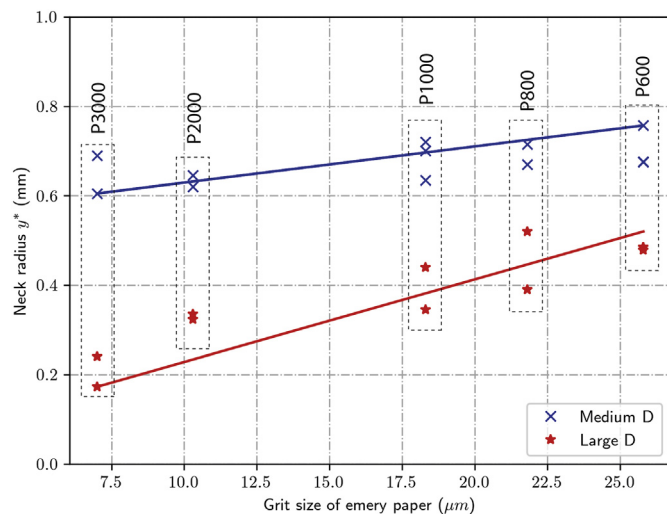


Fig. 13. Comparison of the neck radii of capillary bridges for different surfaces at $D: 0.72\text{mm} \sim 0.75\text{mm}$ (x) and $D: 0.98\text{mm} \sim 1.04\text{mm}$ (*).

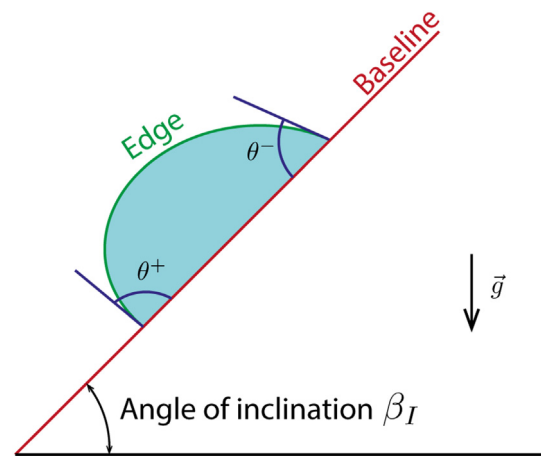


Fig. 14. Advancing (θ^+) and receding (θ^-) contact angles of a deformed droplet on an inclined surface of angle β_I .

The experimental set-up is similar to the capillary bridge test described in Section 3, with the only difference being that the sample is replaced by a controllable rotation platform whose inclination with respect to the plane perpendicular to the image recording direction of the camera is adjustable with the precision of 1° (Fig. 14). It is worth noting that the droplets considered in this test are under a static regime, where the contact points stay fixed throughout the test. All tests were performed under the same controlled laboratory condition (temperature $T = 20^\circ\text{C}$ and relative humidity $H = 55\%$).

Emery papers P600, P800, P1000, P2000 and P3000 were used in the experiments. In each test, a droplet of $V = 15 \mu\text{l}$ was applied to an inclined surface with the angle of inclination β_I . Moreover, the inclination of the baseline was controlled by a rotating platform that can vary β_I from 0° to 55° (starting at 60°, some droplets start to move and the quasi-static regime is lost). The concept of angle of inclination was addressed in [42] where the authors investigated the behavior of a granular mass on an inclined plane. The angle of inclination β_I of the experiments performed in this study is smaller than the critical value $\beta_{I-start}$ that may trigger an avalanche in a granular mass, which is equivalent to the dragging of the droplet on a rough surface. $\beta_{I-start}$ is the value of the angle of inclination at the moment when the granular mass or the droplet starts to move due to the effect of gravity, which can be obtained from experimental observations. Each surface with a glued sand paper was used only once. After the test was completed, a new sample of sand paper was glued on the flat surface to avoid the

impact of any residual water. For each test, the edge of the droplet was obtained by a simple threshold filter in the image processing software. The tangent vector was detected manually using an on-screen overlay protractor.

4.2. Effects of surface roughness on droplet wetting

The results obtained for droplet wetting on surfaces with different roughnesses are presented in Figs. 15 and 16, where the average values of θ^+ and θ^- are plotted in terms of the increasing angle of inclination β_I . Firstly, we observe a logical behavior of advancing and receding angles. When β_I increases from a small to larger value, θ^+ and θ^- have opposite trends: θ^+ increases whereas θ^- decreases.

Fig. 16 presents a comparison of the variations of θ^+ and θ^- for different roughness studies. We recover the same tendency observed in Section 3.3: the rougher the surface, the larger are the contact angles. Indeed, the transition from smooth to rough levels decreases the wettability of the surface. This is accompanied by an increase in the contact angle regardless of the hysteresis phenomenon (advancing and receding wetting angles show a similar behavior). This observation is consistent for both droplets on surfaces and capillary bridges between solids.

Moreover, looking into the details shown in Fig. 16, it is observed that there is a larger difference between P3000 and P2000 with respect to other roughness levels. This is due to the corresponding grit sizes of

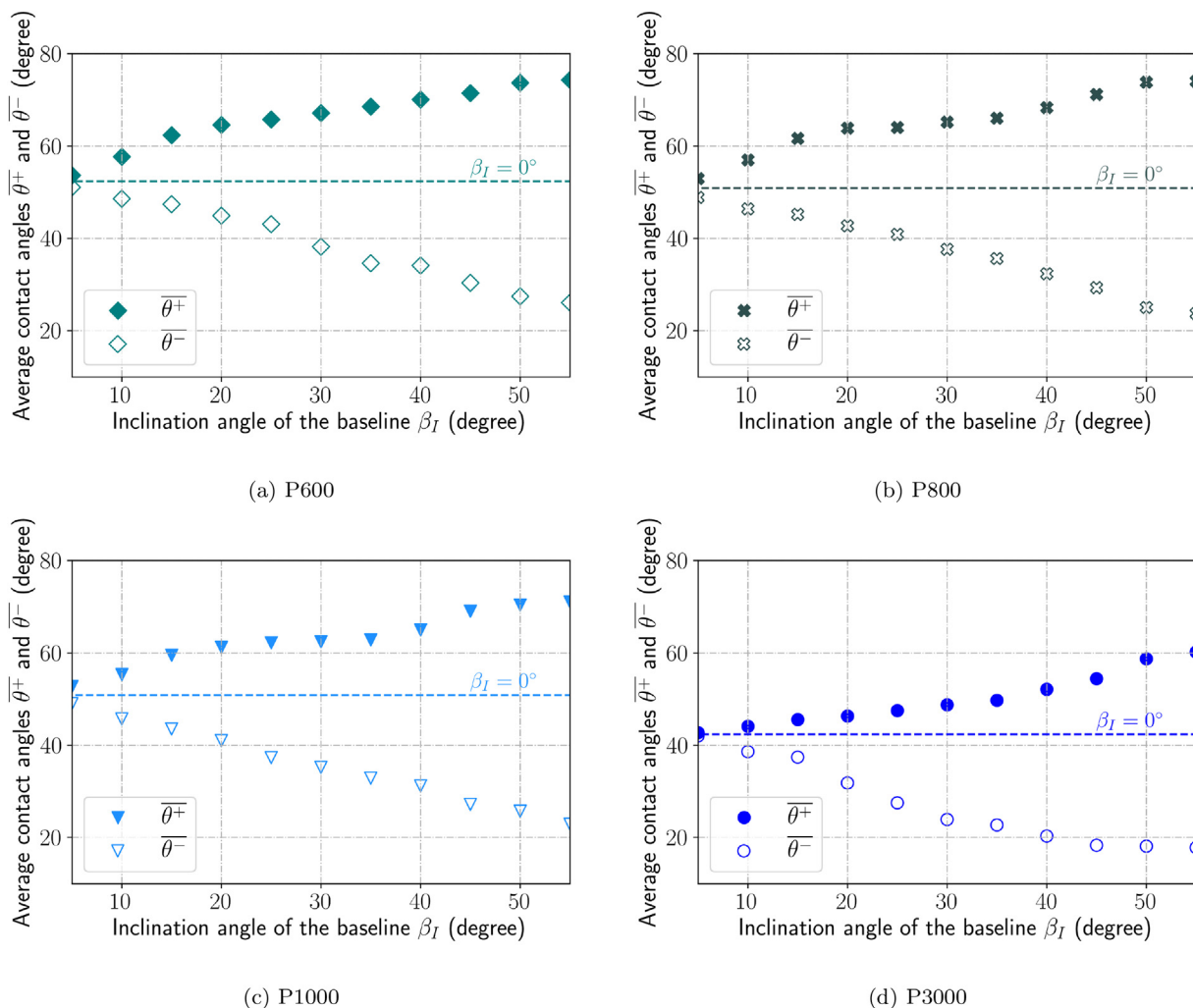


Fig. 15. Variation of contact angles of droplets on inclined surfaces with different roughness levels: (a)(b) Rough surface, P600 and P800, (c)(d) Smooth surface, P1000 and P3000.

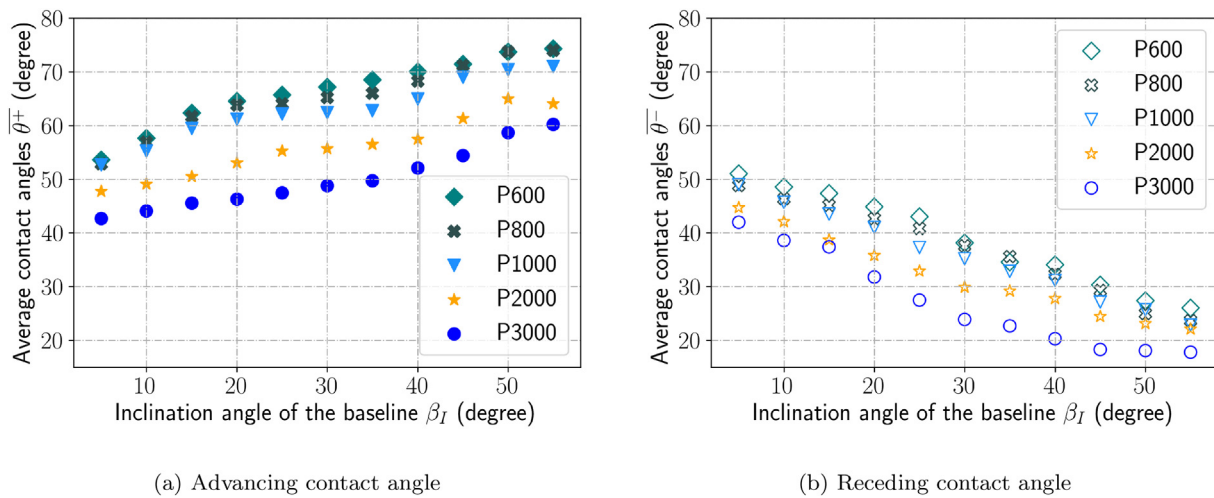


Fig. 16. Comparison between contact angles of droplets on inclined surfaces with different roughness levels.

the sand paper, described in Table 1. Indeed, the average particle diameters of P600, P800, and P1000 are narrower than those of P2000 and P3000.

Comparing to the experimental results reported in [27,28,30–33], where the effect of gravity was not considered, the results of this study show that the effect of gravity does not change the tendency that when the angle of inclination is greater, the advancing angle increases while the receding angle decreases.

5. Conclusions

In this paper, the effects of surface roughness on the capillarity of liquid bridges and the wettability of droplets were experimentally studied. Different surface roughnesses were prepared by gluing waterproof sandpaper onto flat glass surfaces. In the experiments, small volumes of pure water were injected between two parallel plates; thus, the influence of gravity is negligible. Also, large volumes of water droplets on inclined surfaces were investigated.

The effects of surface roughness on liquid bridge capillarity were investigated using a method that is based on an exact analytical solution of the Young-Laplace equation for a liquid bridge between two parallel planes coupled with capillary force measurement. The capillary forces between two parallel planes were measured with a micro-balance, while the geometries of the capillary bridge were recorded using a high resolution camera. From the images of capillary bridges obtained, the meridional profiles of capillary bridges were determined using a high-resolution image processing technique and correlated to the measured capillary forces. Results show that the finer the grit size of the surface, the greater the values of capillary forces that can be achieved. In terms of the geometric description of the capillary bridge, when the roughness of the surface decreases, the mean curvature, the contact radius and neck radius increase. However, the contact angle shows a reverse tendency; it has larger values for rough surfaces and decreases for smoother surfaces. In other words, the roughness amplifies the hydrophobic property of the surface.

In order to demonstrate the impact of the surface roughness on the contact angle, tests of quasi-static droplets on inclined surfaces were performed. The effects of surface roughness on droplet wetting were measured by employing the same high-resolution image processing technique. The measured results show that, as the roughness increases, the wetting angle becomes larger. The transition from smooth to rough levels decreases the wettability of the surface. It was also found that both the advancing and receding wetting angles show a similar behavior.

Declaration of Competing Interest

None.

Acknowledgments

The authors acknowledge support from the international research network GDR-GeoMech (Multi-Physics and Multi-Scale Couplings in Geo-Environmental Mechanics). The authors would also like to express their sincere gratitude to the NEEDS program for having supported this work. The research described was funded in part by the European Union's Horizon 2020 research and innovation program under the Marie Skłodowska-Curie grant agreement No. 832405 (ICARUS) and by the French National Centre for Space Studies (CNES).

References

- [1] E. Riedo, F. Lévy, H. Brune, Kinetics of capillary condensation in Nanoscopic sliding friction, *Phys. Rev. Lett.* 88 (18) (2002), 185505.
- [2] N.P. Krut, O. Millet, An analytical theory for the capillary bridge force between spheres, *J. Fluid Mech.* 812 (2017) 129–151.
- [3] G. Gagneux, O. Millet, Analytic calculation of capillary bridge properties deduced as an inverse problem from experimental data, *Transp. Porous Media* 105 (1) (2014) 117–139.
- [4] A. de Lazer, M. Dreyer, H.J. Rath, Particle-surface capillary forces, *Langmuir* 15 (13) (1999) 4551–4559.
- [5] C.-F. Zhao, N.P. Krut, O. Millet, Capillary bridge force between non-perfectly wettable spherical particles: an analytical theory for the pendular regime, *Powder Technol.* 339 (2018) 827–837.
- [6] C.-F. Zhao, N.P. Krut, O. Millet, Capillary bridges between spherical particles under suction control: rupture distances and capillary forces, *Powder Technol.* 360 (2020) 622–634.
- [7] C.-F. Zhao, N.P. Krut, O. Millet, Capillary bridges between unequal-sized spherical particles: rupture distances and capillary forces, *Powder Technol.* 346 (2019) 462–476.
- [8] F.M. Orr, L.E. Scriven, A.P. Rivas, Pendular rings between solids: meniscus properties and capillary force, *J. Fluid Mech.* 67 (4) (1975) 723–742.
- [9] G. Lian, C. Thornton, M.J. Adams, A theoretical study of the liquid bridge forces between two rigid spherical bodies, *J. Colloid Interface Sci.* 161 (1) (1993) 138–147.
- [10] S.R. Brown, Fluid flow through rock joints: the effect of surface roughness, *Journal of Geophysical Research: Solid Earth* 92 (B2) (1987) 1337–1347.
- [11] E. Bonaccorso, H.-J. Butt, V.S.J. Craig, Surface roughness and hydrodynamic boundary slip of a Newtonian fluid in a completely wetting system, *Phys. Rev. Lett.* 90 (14) (2003), 144501.
- [12] J.B. Taylor, A.L. Carrano, S.G. Kandlikar, Characterization of the effect of surface roughness and texture on fluid flow—past, present, and future, *Int. J. Therm. Sci.* 45 (10) (2006) 962–968.
- [13] R.E. Johnson, R.H. Dettre, D.A. Brandreth, Dynamic contact angles and contact angle hysteresis, *J. Colloid Interface Sci.* 62 (2) (1977) 205–212.
- [14] C.D. Willett, M.J. Adams, S.A. Johnson, J.P.K. Seville, Effects of wetting hysteresis on pendular liquid bridges between rigid spheres, *Powder Technol.* 130 (1) (2003) 63–69.

- [15] T.S. Meiron, A. Marmur, I. Saguy, Contact angle measurement on rough surfaces, *J. Colloid Interface Sci.* 274 (2) (2004) 637–644.
- [16] Z. Shi, Y. Zhang, M. Liu, D.A.H. Hanaor, Y. Gan, Dynamic contact angle hysteresis in liquid bridges, *Colloids Surf. A Physicochem. Eng. Asp.* 555 (2018) 365–371.
- [17] J. Fortin, O. Millet, G. de Saxcé, Mean stress in a granular medium in dynamics, *Mech. Res. Commun.* 29 (4) (2002) 235–240.
- [18] O. Millet, J. Rahmoun, G. de Saxcé, Analytic calculation of the stresses in an ensiled granular medium, *Comptes Rendus Mécanique* 334 (2) (2006) 137–142.
- [19] J. Rahmoun, O. Millet, G.d. Saxcé, A continuous media approach to modeling the stress saturation effect in granular silos, *J. Stat. Mech.* 2008 (06) (2008) P06011.
- [20] J. Rahmoun, D. Kondo, O. Millet, A 3d fourth order fabric tensor approach of anisotropy in granular media, *Comput. Mater. Sci.* 46 (4) (2009) 869–880.
- [21] J. Rahmoun, O. Millet, J. Fortin, Friction effect on stresses in ensiled granular media, *Comput. Geotech.* 36 (7) (2009) 1113–1124.
- [22] H.N.G. Nguyen, F. Prunier, I. Djeran-Maigre, F. Nicot, Kinetic energy and collapse of granular materials, *Granul. Matter* 18 (1) (2016) 5.
- [23] H.N.G. Nguyen, O. Millet, G. Gagneux, Exact calculation of axisymmetric capillary bridge properties between two unequal-sized spherical particles, *Mathematics and Mechanics of Solids* 24 (9) (2019) 2767–2784.
- [24] H.N.G. Nguyen, O. Millet, G. Gagneux, On the capillary bridge between spherical particles of unequal size: analytical and experimental approaches, *Contin. Mech. Thermodyn.* 31 (1) (2019) 225–237.
- [25] H.N.G. Nguyen, O. Millet, G. Gagneux, Liquid bridges between a sphere and a plane—classification of meniscus profiles for unknown capillary pressure, *Mathematics and Mechanics of Solids* 24 (10) (2019) 3042–3060.
- [26] X. Li, M. Dong, H. Zhang, S. Li, Y. Shang, Effect of surface roughness on capillary force during particle-wall impactation under different humidity conditions, *Powder Technol.* 371 (2020) 244–255.
- [27] J.J. Bikerman, The surface roughness and contact angle, *The Journal of Physical and Colloid Chemistry* 54 (5) (1950) 653–658.
- [28] R.N. Wenzel, Surface roughness and contact angle, *J. Phys. Chem.* 53 (9) (1949) 1466–1467.
- [29] Y. Wang, S. Michielsen, H.J. Lee, Symmetric and asymmetric capillary bridges between a rough surface and a parallel surface, *Langmuir* 29 (35) (2013) 11028–11037.
- [30] H.-J. Butt, Capillary forces: influence of roughness and heterogeneity, *Langmuir* 24 (9) (2008) 4715–4721.
- [31] G. Zografi, B.A. Johnson, Effects of surface roughness on advancing and receding contact angles, *Int. J. Pharm.* 22 (2–3) (1984) 159–176.
- [32] D. Kim, N.M. Pugno, S. Ryu, Wetting theory for small droplets on textured solid surfaces, *Sci. Rep.* 6 (2016) 37813.
- [33] K.J. Kubiak, M.C.T. Wilson, T.G. Mathia, P. Carval, Wettability versus roughness of engineering surfaces, *Wear* 271 (3) (2011) 523–528.
- [34] C. Delaunay, Sur la surface de révolution dont la courbure moyenne est constante, *Journal de Mathématiques Pures et Appliquées* (1841) 309–314.
- [35] H.N.G. Nguyen, O. Millet, C.-F. Zhao, G. Gagneux, Theoretical and experimental study of capillary bridges between two parallel planes, *Eur. J. Environ. Civ. Eng.* (2020) 1–11.
- [36] G. Gagneux, O. Millet, B. Mielniczuk, M.S.E. Youssoufi, Theoretical and experimental study of pendular regime in unsaturated granular media, *Eur. J. Environ. Civ. Eng.* 21 (7–8) (2017) 840–853.
- [37] M.J. Adams, S.A. Johnson, J.P. Seville, C.D. Willett, Mapping the influence of gravity on pendular liquid bridges between rigid spheres, *Langmuir* 18 (16) (2002) 6180–6184.
- [38] B. Mielniczuk, O. Millet, G. Gagneux, M.S. El Youssoufi, Characterisation of pendular capillary bridges derived from experimental data using inverse problem method, *Granul. Matter* 20 (1) (2018) 14.
- [39] H.N.G. Nguyen, C.-F. Zhao, O. Millet, G. Gagneux, An original method for measuring liquid surface tension from capillary bridges between two equal-sized spherical particles, *Powder Technol.* 363 (2020) 349–359.
- [40] v. Šikalo, C. Tropea, E.N. Ganić, Impact of droplets onto inclined surfaces, *J. Colloid Interface Sci.* 286 (2) (2005) 661–669.
- [41] P.G. de Gennes, Wetting: statics and dynamics, *Rev. Mod. Phys.* 57 (3) (1985) 827–863.
- [42] O. Pouliquen, Y. Forterre, Friction law for dense granular flows: application to the motion of a mass down a rough inclined plane, *J. Fluid Mech.* 453 (2002) 133–151.